Phys Chem Minerals (1998) 25:574–584

ORIGINAL PAPER

G.V. Gibbs · M.B. Boisen · F.C. Hill · O. Tamada
R.T. Downs

SiO and GeO bonded interactions as inferred from the bond critical point properties of electron density distributions

Received: 18 August 1997 / Revised, accepted: 19 February 1998

Abstract The topological properties of the electron density distributions for more than 20 hydroxyacid, geometry optimized molecules with SiO and GeO bonds with 3-, 4-, 6- and 8-coordinate Si and Ge cations were calculated. Electronegativities calculated with the bond critical point (bcp) properties of the distributions indicate, for a given coordination number, that the electronegativity of Ge ($\sim$1.85) is slightly larger than that of Si ($\sim$1.80) with the electronegativities of both atoms increasing with decreasing bond length. With an increase in the electron density, the curvatures and the Laplacian of the electron density at the critical point of each bond increase with decreasing bond length. The covalent character of the bonds are assessed, using bond critical point properties and electronegativity values calculated from the electron density distributions. A mapping of the (3, –3) critical points of the valence shell concentrations of the oxide anions for bridging SiOSi and GeOGe dimers reveals a location and disposition of localized nonbonding electron pairs that is consistent with the bridging angles observed for silicates and germanates. The bcp properties of electron density distributions of the SiO bonds calculated for representative molecular models of the coesite structure agree with average values obtained in X-ray diffraction studies of coesite and danburite to within $\sim$5%.

Introduction

The crystal chemistry and behavior of silicate and germanate materials are similar, a relationship that stems in part from the fact that Si and Ge atoms have similar ionization potentials and electronegativities (Goldschmidt 1931; Weber 1973). Coupled with this similarity, germanates at ambient conditions have been found to serve as model structures for silicates at high pressures. For example, GeO_2 not only crystallizes at room pressure with the same enantiomorphic framework structures as quartz, SiO_2, but it is also a nearly perfect high-pressure model with the fractional coordinates of its atoms, its tetrahedral and bridging angles and its *c/a* ratio approaching those of quartz at 10 GPa (Glinnemann et al. 1992). In addition, a theoretical study by Silvi et al. (1992) indicates a 'great similarity between cristobalite modifications of SiO_2 and GeO_2.' Not only are the internal coordinates of the atoms in both modifications very similar, but also the high-low transitions exhibited by the two can be described by the same mechanism. In addition to these examples, a relatively large number of germanates have been synthesized that are structurally related to a variety of rock forming silicate minerals (see Goldsmith 1950; McCormack 1964, 1966; McCormack and Ehlers 1967; Miller et al. 1967; Toraya et al. 1978; Navrotsky 1989). Indeed, many are not only structurally related but are also isostructural, having similar physical properties, sometimes exhibiting similar phase relationships and transitions. However, silicates and germanates differ in two important ways: the GeO bond is typically $\sim$0.15 Å longer than the SiO bond while the GeOGe angle is typically narrower than the SiOSi angle by $\sim$15° (Gibbs et al. 1987). These differences can be ascribed, at least in part, to the fact that Ge, a third row cation, is intrinsically larger than a second row Si cation (Shannon and Prewitt 1969) and that the GeO bond is slightly more covalent than the SiO bond with the resulting GeOGe angle adopting a smaller value than that adopted by the SiOSi angle (Silvi et al. 1992). As shown later, the narrower GeOGe angle can also be ascribed to the fact that the bridging oxide anion of a GeOGe dimer exhibits two localized nonbonded lone electron pairs while the bridging oxide anion of the SiOSi dimer exhibits only one.

In spite of these differences, studies of the bonded interactions and the bond lengths and angles reported for

G.V. Gibbs (✉) · M.B. Boisen · F. C. Hill
Departments of Geological Sciences,
Mathematics and Material Science and Engineering, Virginia Tech, Blacksburg, VA 24061, USA

O. Tamada
Graduate School of Human and Environmental Studies,
Kyoto University, Kyoto 606, Japan

R.T Downs
Department of Geological Sciences, University of Arizona, Tucson, AZ, USA

silicate and germanate materials have shown that their *M*O bond lengths, (*R*(*M*O), *M*=Si, Ge), correlate in a similar way with the angles within and between tetrahedral oxyanions with shorter bonds tending to involve wider angles (see Brown et al. 1969; Tossell and Gibbs 1978; Gibbs 1982; Hill et al. 1977; Boisen and Gibbs 1987; Gibbs et al. 1987; Nishi and Takéuchi 1992). Also, potential energy curves calculated as a function of the *M*O bond lengths for hydroxyacid molecules with 4- and 6-coordinated Si and Ge conform with the observed range of SiO and GeO bond lengths reported for crystals (Gibbs 1982; Gibbs et al. 1987). What is more, Mulliken bond overlap populations, *n*(*M*O), calculated for the *M*O bonds for model molecules of coordinated polyhedra cut from silicate and germanate crystals have been observed to correlate with *R*(*M*O) with larger *n*(*M*O) values tending to involve shorter bonds and wider angles (Hill et al. 1977). As a close connection exists between overlap population and the electron density distribution, an inverse relationship is expected to obtain between bond length and the build-up of electron density in the bonds. Theoretical deformation electron density $\Delta\rho(\mathbf{r})$ maps, calculated along the *M*O bonds of silicate and germanate molecules are likewise similar, suggesting that the redistribution of the electron density in formation of the SiO and GeO bonds is similar as well (Gibbs et al. 1987).

Properties of the SiO bonded interactions inferred from $\Delta\rho(\mathbf{r})$ maps

During the past 20 years, experimental $\Delta\rho(\mathbf{r})$ maps have been generated from X-ray diffraction data for a number of silicates. As no such experimental maps were found in a search of the literature for germanates, the following discussion is necessarily restricted to an examination of the maps recorded for silicates.

In a review of the $\Delta\rho(\mathbf{r})$ maps recorded for more than 25 silicates, Tsirelson et al. (1990) concluded, on the basis of the 'smeared' distributions and the heights of the peaks along the SiO bonds, that the bond exhibits a predominant amount of covalent and multiple $(p-d)\pi$ bond character (see also Stuckenschmidt et al. 1994; Smrĉok and Benco 1996). Teppen et al. (1994) reached a similar conclusion in a study of a $\Delta\rho(\mathbf{r})$ map calculated along the SiOSi bond of the $H_6Si_2O_7$ molecule at the MP2/MC6-311G** level. In contrast Cohen (1994) concluded, on the basis of theoretical model $\Delta\rho(\mathbf{r})$ maps calculated by Binggeli et al. (1991), that quartz is 'clearly very ionic' and consists of nearly fully charged Si^{4+} and O^{2-} ions (see also Gillespie and Johnson 1997). These contrasting pictures of the SiO bond conform with the difficulty of establishing a direct link between the height/position of a $\Delta\rho(\mathbf{r})$ peak along a bond and the ionic/covalent character of the bond (Cremer and Kraka 1984a, 1984b; Spackman and Maslen 1985; Cremer 1987). One of the more intractable problems in interpreting $\Delta\rho(\mathbf{r})$-maps is that the reference state promolecule (procrystal) distribution, that is subtracted point by point from the theoretical or experimental electron density distribution of a molecule (crystal), can be constructed in several different ways (Cremer and Kraka 1984a, b; Cremer 1987; Gatti et al. 1992). Actually, except perhaps in special cases, there may be no easy and consistent way of constructing a reference state distribution that accurately reflects the distribution prior to bond formation. To avoid the problem of the reference state, Downs and Swope (1992) and Downs (1994, 1995) undertook studies of the bond critical point (bcp) properties of the total electron density distributions of the SiO bonds for the framework structures danburite, $CaB_2Si_2O_8$, and coesite, a high-pressure polymorph of SiO_2. In addition, Gibbs et al. (1994; 1997), Hill et al. (1997) and Gillespie and Johnson (1997) undertook similar studies of the bcp properties of the SiO bonds for a variety of hydroxyacid and siloxane molecules. In these studies, the strategies and bcp criteria devised by Bader and Essén (B&E) (1984) were employed in studying bonded interactions and bond type (see also Bader 1990). Despite the absence of experimental $\Delta\rho(\mathbf{r})$ maps for the GeO bond, total valence electron density maps have been calculated in a careful pseudopotential periodic Hartree-Fock study of SiO_2 and GeO_2 modifications of cristobalite. In the study, Silvi et al. (1992) found that the valence electrons are mainly concentrated in the vicinity of the oxide anions with bulges directed along the bonds much like that observed for coesite (Jackson and Gibbs 1988). They concluded upon subtracting the total valence electron density distribution of the SiO_2 modification from that of GeO_2 modification that the GeO bond is slightly more covalent that the SiO bond.

Criteria for defining bonded interactions from bond critical point properties

With the B&E criteria, it is possible to define a continuum of interactions between different pairs of bonded atoms ranging between a closed-shell ionic interaction at one extreme and a shared covalent interaction at the other. In the case of a closed-shell polar interaction, the value of the electron density, $\rho(\mathbf{r}_c)$ at the (3, −1) bond critical point, $\mathbf{r}_c$, is pictured as being relatively small. The two orthogonal curvatures ($|\lambda_1|$ and $|\lambda_2|$) of $\rho(\mathbf{r}_c)$ measured perpendicular to the bond path (λ_1 and λ_2 are the eigenvalues of the Hessian of $\rho(\mathbf{r})$ at $\mathbf{r}_c$ associated with a pair of mutually perpendicular eigenvectors oriented perpendicular to the path) are likewise pictured as being relatively small while the curvature, λ_3 of $\rho(\mathbf{r}_c)$ measured parallel to the path (λ_3 is the third eigenvalue of the Hessian associated with an eigenvector that parallels the bond path at $\mathbf{r}_c$) is pictured as being relatively large. Since λ_1 and λ_2 are both relatively small and negative in value and λ_3 is pictured as being positive and larger in value, this results in a positive and a relatively large value for the Laplacian of $\rho(\mathbf{r}_c)$ ($\nabla^2\rho(\mathbf{r}_c)=\lambda_1+\lambda_2+\lambda_3$) and a value less than unity for the ratio $|\lambda_1|/\lambda_3$. On the other hand, for a shared covalent interaction, the values of $\rho(\mathbf{r}_c)$, $|\lambda_1|$ and $|\lambda_2|$ are pictured as being relatively large while λ_3 is pictured as relatively small,

resulting in a negative value for the Laplacian and a $|\lambda_1|/\lambda_3$ ratio greater than unity. Thus, when an assortment of polar covalent bonds are considered, they are pictured as exhibiting a range of properties between the two extremes.

Properties of the SiO bonded interactions inferred from bond critical point criteria

In an application of the B&E criteria to the bonded interactions in danburite and coesite, Downs (1995) concluded that the SiO bond is polar covalent in conformity with earlier proposals made by Pauling (1940). The values of $\rho(\mathbf{r}_c)$ for the SiO bonds observed for these minerals range between 0.94 e/Å^3 and 1.16 e/Å^3, with an average value of 1.02 e/Å^3, compared with an average value of $\sim$0.55 e/Å^3 observed for the polar BeO bond in bromellite, BeO, (Downs 1991) and $\sim$3.0 e/Å^3 calculated for the predominately covalent CO bond (Hill et al. 1997). In addition, the distance between the oxide anion and the minimum in $\rho(\mathbf{r})$ along each of the SiO bonds (i.e., the bonded radius of the oxide ion, r_b(O), measured along the bond path) decreases with decreasing bond length. Concomitant with these changes, λ_3 and $\nabla^2\rho(\mathbf{r}_c)$, tend to increase in magnitude as the observed SiO bond decreases in length. The observation that the value of r_b(O) decreases with decreasing bond length suggests that the covalent character of the SiO bond increases with decreasing bond length (Bader 1990). But, the increase in both λ_3 and $\nabla^2\rho(\mathbf{r}_c)$ for both coesite and danburite with decreasing R(SiO) is in conflict with the B&E criteria with the covalent character of the SiO bond indicated to decrease as the SiO bond shortens. However, the values of $\rho(\mathbf{r}_c)$ and the curvatures $|\lambda_1|$ and $|\lambda_2|$ are each observed to be essentially randomly scattered when plotted against R(SiO), providing little insight into how the character of the bond changes with bond length. Nonetheless, the observation (1) that the $|\lambda_1|/\lambda_3$ ratio is less than unity and ranges between 0.20 and 0.25 and (2) that $\nabla^2\rho(\mathbf{r}_c)$ is positive and relatively large in value (ranging between 17 to 22 e/Å^5) indicates (B&E criteria) that the SiO bond is highly polar and ionic in character.

In a parallel study, the bcp properties were calculated for several small $H_6Si_2O_7$ molecular models of the coesite structure at the Hartree-Fock level, using a 6-311++G** basis set (Gibbs et al. 1994). With the bond lengths and angles of the $Si_2O_7^{6-}$ anion of each model fixed at the values observed for coesite, it was found (as observed for the danburite and coesite data sets) that with decreasing SiO bond length, r_b(O) decreases while λ_3 and $\nabla^2\rho(\mathbf{r}_c)$ both increase in value. In contrast with the experimental data set, it was found that the value of $\rho(\mathbf{r}_c)$ and its associated curvatures measured perpendicular to the bond each increase with decreasing SiO bond length (Gibbs et al. 1994). Again, several of the theoretical trends are in conflict with the B&G criteria.

In addition to these conflicting trends, it is important to note that the absolute magnitudes of the bcp properties calculated for the $H_6Si_2O_7$ models are $\sim$15% smaller than those observed for the danburite and coesite data sets. This observation indicates that either the molecular orbital calculations employed in the study are relatively inaccurate, that the molecules used to model the coesite structure are too small or that the experimental data may contain systematic errors such as extinction effects.

Goals and scope of study

In this study, bcp properties were calculated for larger and more representative $H_{12}Si_5O_{16}$ molecular models of the coesite structure, using the more accurate Becke3LYP/6-31G(2d,p) method. As will be discussed in more detail later, the properties obtained in these calculations were found to be in reasonable agreement with those observed for coesite. Becke3LYP/6-31G(2d,p) level calculations were likewise completed for the smaller $H_6Si_2O_7$ molecule. As these calculations yielded results that are virtually the same as those obtained for the larger molecules, it was concluded that the lack of agreement obtained in the earlier calculations can be either ascribed in large part to the poorer accuracy of 6-311++G** basis set calculations rather than to the smaller size of the molecule or to systematic errors in the observed electron density distributions.

Encouraged by the improved agreement, Becke3LYP/6-31G(2d,p) level calculations were also completed for more than 20 geometry optimized hydroxyacid silicate and germanate molecules with the goals of exploring how the bcp properties of the SiO and GeO bonds for these molecules relate to one another and how they vary with bond length. A comparison of the properties was expected to improve our picture of how the electron density in the internuclear region between each pair of bonded atoms is redistributed with changes in bond length, coordination number and multiple bonding and how these changes relate to the electronegativities of Si and Ge. The calculations were also expected to shed light on the conflicting trends presented between bond length and the bcp properties. Finally, the bonded interactions comprising the SiO and GeO bonds will be assessed in terms of the B&E criteria, the local energy density criteria of Cremer and Kraka (1984b), C&K (see later) and the electronegativities of Si and Ge.

Calculations

As indicated in the last section, Becke3LYP/6-311G(2d,p) level calculations were completed on $H_{12}Si_5O_{16}$ molecular models (Frisch et al. 1993). This level of calculation includes some of the effects of electron correlation and exchange and is not only more accurate but faster than calculations completed at the MP2/6-311G(2d,p) level (Foresman and Frisch 1996). As observed by Cremer et al. (1988), two sets of d-type polarization functions (as adopted in this study) are required to model accurately the electron density distributions for Si-containing molecules. This may explain why 6-311++G** basis calculations sporting only one set of *d*-type polarization functions yielded bcp properties for the $H_6Si_2O_7$ molecules that are $\sim$15% smaller than those observed for danburite and coesite. However, experience has shown that Becke3LYP-type calculations tend to underestimate the density at the core region of each atom in a molecule and to overestimate it somewhat in the binding regions. This parallels the fact that the diagonal elements of the Fock matrix obtained in such calculations are often too small (D. Cremer personal communication). Hence, some of the improvement in the bcp properties may reflect this defect in the model. The bcp data were calculated with the AIMPAC series of programs (Biegler-König et al. 1982) which were modified to handle the relatively large number of the wave functions and primitives comprising the basis functions for large molecules like $H_{12}Si_5O_{16}$.

As in earlier calculations, the bond lengths and angles of two $Si_5O_{16}^{12-}$ anions (one centered on the Si_1 atom and the other on the Si_2 atom in coesite) were fixed at the values observed for coesite.

Both anions were charge balanced by attaching a proton to each of the terminal oxide anions at a distance of 1.0 Å to form two models of $H_{12}Si_5O_{16}$ composition with straight SiOH angles. In addition to charge balancing the anions, the protons were assumed to mimic the crystal field of the remaining atoms in the coesite structure.

A comparison of observed and calculated bond critical point properties

The bcp properties calculated for the central Si_1O_4 and Si_2O_4 tetrahedra of both $H_{12}Si_5O_{16}$ molecular models show the same trends with SiO bond length as reported by Gibbs et al. (1994) for the smaller $H_6Si_2O_7$ models: with decreasing SiO bond length, $\rho(\mathbf{r}_c)$, $|\lambda_1|$ $|\lambda_2|$ and λ_3 each increases in value. But, unlike the earlier calculations, the magnitudes of the average bcp properties calculated for the models are in closer agreement with the values observed,

	r_b(O) (Å)	$\rho(\mathbf{r}_c)$ (e/Å^3)	λ_1 (e/Å^5)	λ_2 (e/Å^5)	λ_3 (e/Å^5)	$\nabla^2\rho(\mathbf{r}_c)$ (e/Å^5)
$H_{12}Si_5O_{16}$	0.94	1.01	−7.4	−7.3	35.9	21.1
observed	0.94	1.02	−7.4	−6.9	33.9	19.6
$H_6Si_2O_7$	0.94	1.00	−7.4	−7.3	35.6	20.9

on average, for coesite and danburite. To learn whether this agreement can be ascribed to the larger size of the $H_{12}Si_5O_{16}$ models or to the more accurate level of the calculation, the geometry of a $H_6Si_2O_7$ molecule (C_v point symmetry) was optimized at the Becke3LYP/6-311G(2d,p) level with its OH bonds directed away from the terminal oxide anions to avoid the formation of bonds between the H atoms and the terminal oxide anions of the adjacent SiO_4 group of the dimer (Burkhard et al. 1991). The resulting structure has SiO(br) bond lengths of 1.615 Å and an SiOSi angle of 145.0º. As the bcp properties of the bridging SiO bonds are nearly the same as those obtained, on average, for the two larger models it is apparent that the improvement is more dependent on the level of the calculation than on the size of the molecular model. We note in passing that the bonded radius of the oxide anion of 0.94 Å obtained on average in the calculations and from the experimental maps for coesite and danburite is significantly smaller than that (1.28 Å) obtained from an MP2 electron density distribution calculated for the $H_6Si_2O_7$ molecule (Teppen et al. 1994).

A potential energy surface for the SiOSi disiloxy unit

Inasmuch as the bcp properties of the SiOSi disiloxy unit of the $H_6Si_2O_7$ molecule agree to within ~5% with those observed, on average, for coesite and danburite and as a close connection exists between the geometry of a bonded system and its electron density distribution, a potential energy surface was generated for the molecule as a function of its bridging SiO bond length, R(SiO), and the SiOSi angle (Fig. 1). This calculation was undertaken to see how well the bond lengths and SiOSi angles observed for the

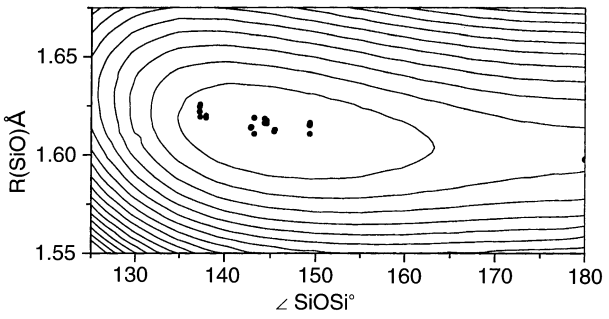

Fig. 1 A potential energy surface for the $H_6Si_2O_7$ molecule (C_v point symmetry) calculated as a function of the SiO bridging bond length, *R*(SiO), and the SiOSi angle with all of the other internal coordinates of the molecule fixed at their geometry optimized values. The level lines were drawn at intervals of 2 kJ/mole. Superimposed on the plot are bond length and angle data observed for the silica polymorphs quartz, cristobalite and coesite. The observed bond length data were corrected for thermal motion effect (Downs et al. 1992). The optimized SiO bond length and SiOSi angle calculated for the molecule are 1.615 Å/ and 145.0º, respectively

silica polymorphs correspond with a surface calculated for a small and relatively simple $H_6Si_2O_7$ molecule at the Becke3LYP/6-311G(2d,p) level. In the calculations, the only internal coordinates of the molecule that were varied from the geometry optimized values were the SiOSi angle and the bridging SiO bonds. As both of these bonds were calculated to be identical in length, they were constrained to be equal in length in the calculation of the surface. The topography of the surface, displayed in Fig. 1, is similar to one calculated earlier with a relatively crude STO-3G basis set (Gibbs et al. 1981). The SiO bond lengths, R(SiO), and the associated SiOSi angle data observed for the silica polymorphs coesite, quartz and cristobalite are plotted on the surface. The bond length data for these materials were corrected for the effects of thermal motion using the strategies devised by Downs et al. (1992). The data not only follow the trend of the valley floor of the surface, but the bulk of the bond length and angle data cluster to within ~2 kJ/mol of the energy of the optimized geometry. The SiO bond comprising the straight angle in coesite is indicated to destabilize a structure by only about ~3 kJ/mol. The bond length and angle data recorded for the silica polymorphs are in better agreement with this surface than they are with one calculated at the STO-3G level. See Gibbs (1982) and Gibbs and Boisen (1998) for a discussion of the surface, the compliance of the SiOSi angle and the implications of the surface in terms of why silica is a good glass former, why there are such a large number of different structure types for silica and silicates and why silica polymorphs like quartz display relatively high compressibilities. The good agreement obtained between the observed and calculated bond lengths, angles and bcp properties for coesite suggests that Becke3LYP/6-311G(2d,p) level calculations can yield accurate properties, as carefully documented by Foresman and Frisch (1996). It also supports the argument that the local force field and the electron density distribution of an SiOSi dimer play a determinental role in

governing the structures of the silica polymorphs with 4-coordinate Si (Gibbs 1982). A recent photon diffraction study of the bond angle distributions in amorphous silica and germania (Neuefeind and Liss 1996) yielded average SiOSi and GeOGe angles of 148.3º and 133.0º, respectively, in close agreement with the geometry optimized angle (149.0º) displayed in Fig. 1 and the geometry optimized GeOGe angle (135.6º) calculated for the $H_6Ge_2O_7$ molecule at the Becke3LYP/6-311G(2d,p) level. However, at variance with the low lying and flat nature of the valley floor (Fig. 1) and the flat nature of the GeOGe potential energy curve calculated for the H_6Ge_2O molecule (Gibbs et al. 1987), the photon diffraction experiments indicate that the SiOSi and GeOGe angle distributions are fairly narrow (σ(<SiOSi)=7.5º; σ(<GeOGe)=8.3º) in amorphous silica and germania (Neuefeind and Liss 1996) unlike the relatively wide range of angles observed for silicate and germanate crystals (Gibbs et al. 1987).

Bond critical point properties for SiO and GeO bonded interactions

Encouraged by the agreement between the observed and calculated geometries and bcp properties, the geometries and electron density distributions were calculated for a variety of hydroxyacid silicate and germanate molecules with 3-, 4-, 5-, 6- and 8-coordinate Si and Ge. The non-equivalent geometry optimized SiO and GeO bond lengths calculated for each molecule are given in Table 1 along with the bcp properties for each of the *M*O bonds. The point symmetry assumed in the calculations for each molecule is given in Table 1. The terminal SiOH and GeOH bonds are denoted as SiO–H and GeO–H, respectively, whereas the bridging bonds comprising corner sharing coordination polyhedra are denoted as SiO_{br} and GeO_{br}. The SiO and GeO double bonds in the molecules H_2SiO_3 and H_2GeO_3 are denoted SiO and GeO, respectively.

The bcp properties of the *M*O bonds calculated for the molecules are plotted in Fig. 2 against the minimum ener-

Table 1 The properties of SiO and GeO bonds in hydroxyacid silicate and germanate molecules

Molecule	*M*O	$R(MO)$ Å	r_b(O) Å	$\rho(\mathbf{r}_c)$ e/Å^3	$\lambda_{1,2}$ e/Å^5	λ_3 e/Å^5	$\nabla^2\rho(\mathbf{r}_c)$ e/Å^5	$H(\mathbf{r}_c)$ H/Å^3
H_4SiO_4 (C_4)	SiO–H	1.676	0.991	0.9139	–6.053	28.336	16.232	–0.445
H_2SiO_3 (C_{2v})	SiO	1.515	0.878	1.307	–8.253	49.944	33.439	–0.721
	SiO–H	1.619	0.951	1.022	–7.265	35.281	20.751	–0.493
$H_8Si_4O_4$ (C_{4h})	SiO_{br}	1.634	0.957	0.924	–6.519	32.484	19.447	–0.381
$H_4Si_4O_6$ (C_{2v})	SiO_{br}	1.678	0.994	0.911	–5.922	28.231	16.387	–0.439
	SiO–H	1.646	0.968	0.939	–6.600	31.267	18.148	–0.430
H_4SiO_4 (S_4)	SiO–H	1.637	0.965	0.987	–7.076	33.291	19.139	–0.477
F_6Si_2O (C_1)	SiO_{br}	1.611	0.943	1.002	–7.322	35.507	20.864	–0.466
$H_{12}Si_6O_6$(C_{6h})	SiO_{br}	1.628	0.953	0.931	–6.627	33.307	20.054	–0.379
$H_6Si_3O_9$(C_{3h})	SiO_{br}	1.639	0.964	0.951	–6.733	32.093	18.628	–0.442
$H_{12}SiO_8$(O_h)	SiO–H	2.009	1.204	0.489	–1.821	6.313	2.672	–0.238
$H_4Si_2O_6$(C_{2h})	SiO–H	1.624	0.956	1.017	–7.316	34.660	20.134	–0.499
	SiO_{br}	1.673	0.991	0.925	–6.115	28.896	16.667	–0.453
H_6Si_2O(C_1)	SiO_{br}	1.646	0.946	0.697	–4.014	21.854	13.827	–0.136
$H_{10}SiO_5$(C_{4h})	SiO_{br}	1.628	0.953	0.927	–6.594	33.186	19.998	–0.374
Cl_6Si_2O(C_1)	SiO_{br}	1.620	0.9484	0.968	–6.825	34.011	20.363	–0.424
H_8SiO_6(O_h)	SiO–H	1.742	1.039	0.801	–4.547	22.310	13.216	–0.389
H_4GeO_4(S_4)	GeO–H	1.768	0.935	0.996	–5.433	25.443	14.577	–0.432
$H_4Ge_2O_6$(C_{2h})	GeO_{br}	1.810	0.959	0.930	–4.770	21.337	11.797	–0.421
	GeO–H	1.754	0.926	1.031	–5.688	26.668	15.291	–0.456
	GeO–H	1.762	0.931	1.008	–5.501	25.892	14.891	–0.439
H_2GeO_3(C_{2v})	GeO	1.642	0.844	1.312	–6.938	35.604	21.729	–0.671
	GeO–H	1.755	0.926	1.021	–5.562	26.428	15.306	–0.444
$H_8Ge_2O_8$(C_s)	GeO_{br}	2.016	1.073	0.563	–2.446	10.811	5.919	–0.192
	GeO_{br}	1.794	0.950	0.908	–4.718	24.548	15.114	–0.315
	GeO–H	1.758	0.929	0.996	–5.238	27.620	17.143	–0.363
	GeO–H	1.836	0.976	0.835	–4.143	20.901	12.616	–0.291
	GeO_{br}	1.932	1.031	0.674	–3.175	14.894	8.544	–0.234
$H_{12}GeO_8$(O_h)	GeO–H	2.054	1.092	0.566	–2.337	9.228	4.553	–0.219
$H_7Ge_2O_7$(C_s)	GeO_{br}	1.755	0.924	0.988	–5.390	26.983	15.52	–0.409
	GeO–H	1.753	0.926	1.036	–5.747	26.874	15.38	–0.459
	GeO–H	1.779	0.941	0.968	–5.221	24.424	13.98	–0.413
$Ge_2O_6H_4$ (C_s)	GeO_{br}	2.108	1.115	0.490	–2.002	7.742	3.739	–0.163
	GeO–H	1.779	0.942	0.983	–5.325	24.510	13.861	–0.433
	GeO–H	1.791	0.949	0.951	–5.072	23.101	12.958	–0.410
	GeO–H	1.811	0.960	0.907	–4.726	21.439	11.988	–0.384
	GeO–H	1.702	0.888	1.167	–6.159	30.306	17.988	–0.572
	GeO–H	1.744	0.918	1.048	–5.723	26.998	15.552	–0.465
H_8GeO_6(O_h)	GeO–H	1.840	0.979	0.866	–4.131	20.097	11.836	–0.395

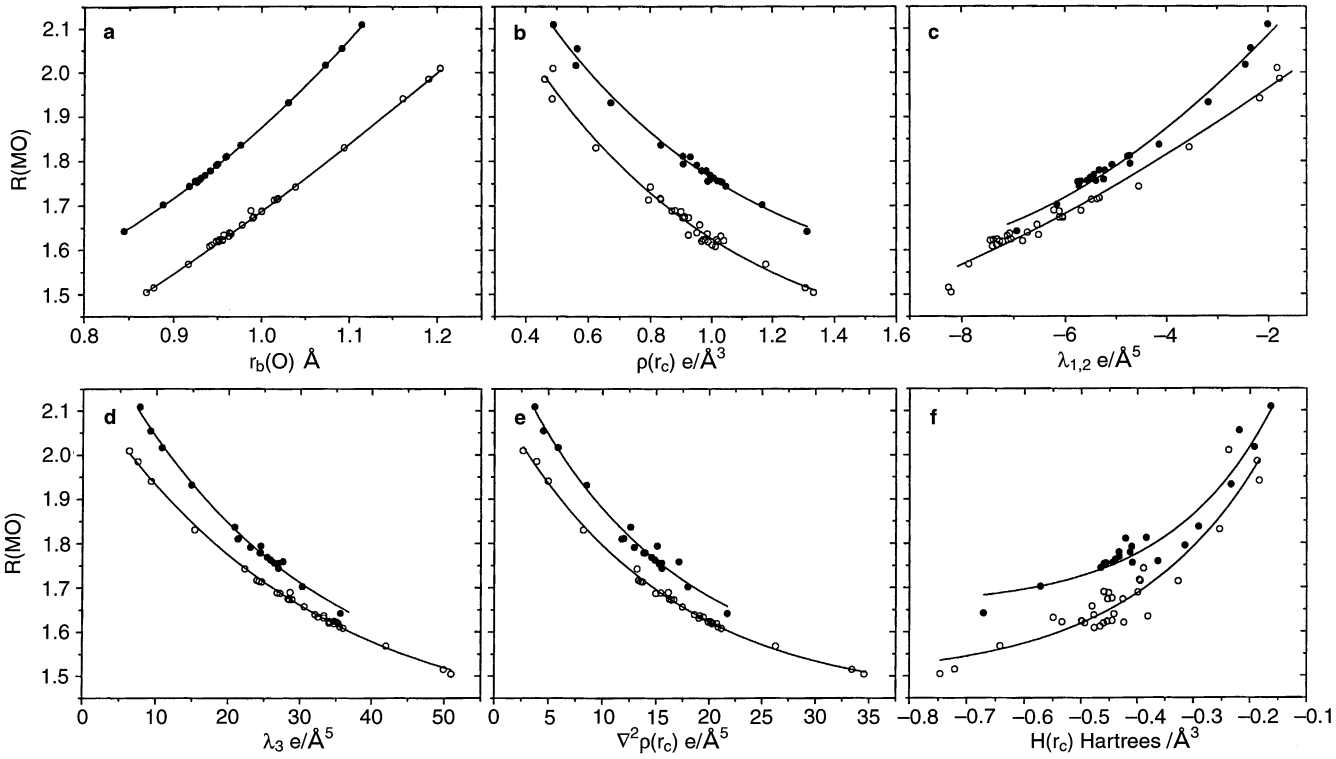

Fig. 2a–f Scatter diagrams of geometry optimized *M*O bond lengths (*M*=Si, Ge) calculated for the molecules in Table 1 versus **a** the bonded radius of the oxide anion, r_b(O), **b** the value of the electron density at the bond critical point, $\mathbf{r}_c$, **c** the average curvature, $\lambda_{1,2}$, of the electron density measured perpendicular to the bond path at $\mathbf{r}_c$, **d** the curvature, λ_3, of the electron density measured parallel to the bond path at $\mathbf{r}_c$, **e** the Laplacian of the electron density, $\nabla^2\rho(\mathbf{r})$, evaluated at $\mathbf{r}_c$ and **f** the local energy density distribution evaluated at $\mathbf{r}_c$. The *open circle* data points denote SiO bond length data and the *closed circle* data points denote GeO bond length data

gy bond lengths, *R*(*M*O). As *R*(*M*O) decreases in value, the SiO and GeO bcp data tend to fall along roughly parallel trends with $\rho(\mathbf{r}_c)$, λ_3 and $\nabla^2\rho(\mathbf{r}_c)$ each increasing in value while r_b(O), $\lambda_{1,2}=1/2(\lambda_1+\lambda_2)$ and $H(\mathbf{r}_c)$ each decrease in value. Thus, with decreasing bond length, there is a progressive build-up of electron density at $\mathbf{r}_c$ accompanied by an increase in the average curvature of the electron density perpendicular to the bond path together with an increase in the curvature of the electron density parallel to the path. In addition, as the ratio r_b(O)/*R*(*M*O) decreases with decreasing bond length, the charge on the oxide ion is indicated to decrease with decreasing bond length (the critical point moves relatively closer to the oxide anion). The systematic increase in the value of λ_3 with decreasing bond length has been argued by Bader (1990) to impart a systematic increase in the 'stiffness' to the bond. Thus, with decreasing bond length, the force constant of the bond is expected to increase as documented by Hill et al. (1994) for the SiO bond.

The increase in the value of $\rho(\mathbf{r}_c)$, the decrease in r_b(O) and the increase in the curvatures of $\rho(\mathbf{r})$ perpendicular to the SiO and GeO bonds are consistent with an increase in the shared interaction component of the bonds (B&E criteria) as both bonds decrease in length. Conversely, the increase in λ_3, the decrease in the $|\lambda_1|/\lambda_3$ ratio from ~0.30 to ~0.15 and the increase of $\nabla^2\rho(\mathbf{r}_c)$ from ~2 to 35 e/Å^5 with decreasing bond length is consistent with an increase in the closed-shell component of the bonds. Indeed, the relatively large $\nabla^2\rho(\mathbf{r}_c)$-values (~35 e/Å^5) calculated for the double bonds of the H_2SiO_3 and H_2GeO_3 molecules are similar to the positive $\nabla^2\rho(\mathbf{r}_c)$-values calculated for the covalently bonded molecules O_2 (12.3 e/Å^5) and CO (41.5 e/Å^5), which also exhibit bcp properties that conflict with the B&E criteria (Cremer and Kraka 1984b; Kraka and Cremer 1990). Thus, despite the improved level of the calculations, conflicting results remain and the picture that $\nabla^2\rho(\mathbf{r}_c)$ decreases in value with increasing covalency does not hold for SiO and GeO bonded interactions. In fact, as shown by Hill et al. (1997) and Feth et al. (1998), it does not hold in general for the bonds in a variety of oxide and nitride molecules containing first and second row main group *M*-cations.

Bonded interactions inferred from local energy density criteria

As the $\nabla^2\rho(\mathbf{r}_c)$ values for the O_2 and CO molecules are each positive, Cremer and Kraka (1984b) (C&K) have questioned whether the B&E criteria that $\nabla^2\rho(\mathbf{r}_c)$ be negative is sufficient for the detection of all shared covalent bonds. To remedy the problem, they used the local energy density, $H(\mathbf{r}_c)=G(\mathbf{r}_c)+\mathcal{V}(\mathbf{r}_c)$, as an indicator of bonded interactions where $G(\mathbf{r}_c)$ is the local kinetic energy density and $\mathcal{V}(\mathbf{r}_c)$ the local potential energy density both evaluated at $\mathbf{r}_c$. In a study of the bcp properties of a number of

molecules, including the two diatomic molecules discussed already, Cremer and Kraka (1984b) suggested that shared covalent interactions are characterized by a predominance of local potential energy density $\mathcal{V}(\mathbf{r}_c)$ at $\mathbf{r}_c$, requiring that $H(\mathbf{r}_c)$ be negative in sign, the more negative the value of $H(\mathbf{r}_c)$, the more covalent the bond (Cremer and Kraka 1984b; Kraka and Cremer 1990). When $H(\mathbf{r}_c)$ is negative in sign, an accumulation of electron density at $\mathbf{r}_c$ is indicated to stabilize a shared covalent interaction. For closed-shell ionic bonded interactions, they found that $H(\mathbf{r}_c)$ tends to be positive, implying that an accumulation of electron density at $\mathbf{r}_c$ results in a destabilization of a molecule upon bond formation. On the other hand, if $H(\mathbf{r}_c)$ is negative, then a bonded interaction is considered to be covalent, the more negative the value of $H(\mathbf{r}_c)$ and the greater the build-up of electron density at $\mathbf{r}_c$, the greater the stabilization of the molecule upon bond formation and the more covalent the bond. In contrast, if $H(\mathbf{r}_c)$ is positive, then a bond is considered to be a polar ionic bond. For this case, one cannot expect a clear cut connection between the character of an ionic bond and the value of $H(\mathbf{r}_c)$ because electrostatic rather than covalent interactions predominate (D. Cremer personal communication). As observed by MacDougall (1989), the local energy density is not a unique parameter and as such can result in ambiguous and conflicting results.

The local energy densities, $H(\mathbf{r}_c)$, are negative for all of the SiO and GeO bonds of the molecules in Table 1. Also, as $R(MO)$ decreases in value, $H(\mathbf{r}_c)$ decreases in value from $\sim$–0.2 to $\sim$–0.8 Hartrees/Å^3, indicating that the SiO and GeO bonds are covalent bonds (C&K criteria) with the covalent character of these bonds increasing with decreasing bond length (Fig. 2f). As there is a progressive build-up of electron density at $\mathbf{r}_c$ as $H(\mathbf{r}_c)$ decreases, it suggests that the molecules are progressively stabilized upon bond formation with decreasing bond length (Cremer and Kraka 1984b). Similar results have been reported for a number of oxide and nitride molecules (Hill et al. 1997; Feth et al. 1998). Collectively, these results and those reported here show that the picture that $\nabla^2\rho(\mathbf{r}_c)$ decreases and becomes negative as bonded interactions change from a closed shell to a shared interaction does not hold for oxides and nitrides, particularly when relatively large changes in bond length are involved.

Electronegativity and bond critical point properties

Our next goal was to learn how the SiO and GeO bond lengths and bcp properties calculated for the molecules in Table 1 correlate with the electronegativities of Si and Ge. It has been demonstrated for a relatively large number of oxide and nitride molecules containing main group M atoms (Hill et al. 1997; Feth et al. 1998) that the electronegativities of each M-atom, χ_M, in the molecules can be estimated with the expression

$$\chi_M = 1.31\,F_M^{-0.23} \qquad (1)$$

F_M=$r_b(X)/(N_M\times\rho(\mathbf{r}_c))$, $r_b(X)$ is the bonded radius of the anion, X, and N_M is the number of valence electrons on M (an equation derived by Boyd and Edgecombe 1988, and modified by Hill et al. 1997). The χ_M-values obtained with this expression for the diatomic molecules studied by Boyd and Edgecombe (1988) agree to within $\sim$1%, on average, with Pauling's thermochemical electronegativities. In addition, the χ_M -values calculated from the bcp properties of the oxides typically match Pauling's electronegativities to within $\sim$5 percent, on average (Hill et al. 1997). For example, the average electronegativity calculated for Li, Na, Al, Si and P agree with Pauling's (1940) values to within $\sim$2% while those calculated for Be, B, C, N, Mg and S tend to differ by $\sim$10%. The value calculated for Si, 1.81, was found to be in close agreement with Pauling's (1940) value (1.8) (Hill et al. 1997). Indeed, χ_M-values estimated using Eq. 1 for Ca (0.97), Be (1.32), B (1.71) Si (1.81) and C (2.99) and the experimental bcp properties of the MO bonds in danburite (Downs and Swope 1992), bromellite (Downs 1991) and L-alanine (Gatti et al. 1992) likewise agree to within $\sim$10%, on average, with Pauling's (1940) values. In a study of partitioned electron density distributions and charge transfer, Maslen and Spackman (1985) have also documented that a close connection exists between Pauling's electronegativity values and the properties of the electron density distributions for a variety of diatomic molecules. Albeit not perfect, the agreement between Pauling's electronegativities and those generated from the bcp properties calculated for hydrides, oxides and nitrides serves to support the Boyd and Edgecombe (1988) suggestion that electronegativities obtained from bcp properties can provide reasonable estimates of the electronegativities of the cations in both molecules and crystals, despite the fact that χ_M is based on a local and not a global property of a bond.

Electronegativity variations of Si and Ge with bond length, coordination number, and multiple bond character

The electronegativity χ_M-values calculated with the bcp properties for the SiO and GeO bonds with Eq. 1 are plotted against $R(MO)$ in Fig. 3a where trends indicate that χ_M for Si and Ge both increase with decreasing bond length and coordination number. Pauling (1940) derived the electronegativities 1.8 and 1.7 for Si and Ge, respectively, while Allen (1989, 1994) derived a smaller electronegativity for Si (1.92) than for Ge (1.99), using the average ionization potentials of the valence-shell electrons of the two atoms.

To learn how the electronegativities of these two atoms vary with bond length and coordination number, calculations were completed for the molecules H_4MO_4 (S_4 point symmetry), H_8MO_6 and $H_{12}MO_8$ (both O_h point symmetry) (Table 1) where the coordination numbers of both Si and Ge increase from 4 to 6 to 8, respectively. As expected, the minimum energy bond lengths calculated for these molecules increase with increasing coordination

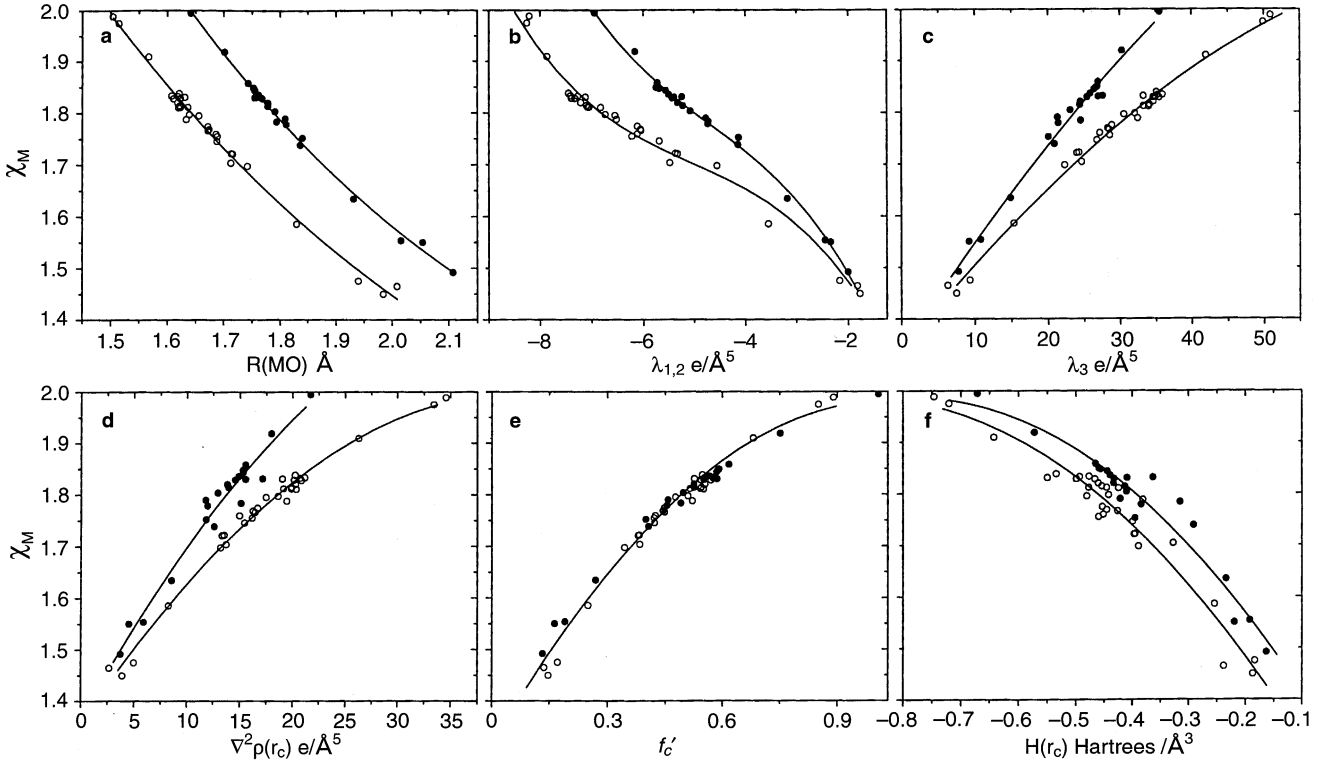

Fig. 3a–f Scatter diagrams of the electronegativties, χ_M, for M=Si and Ge plotted versus **a** the geometry optimized MO bond lengths, $R(MO)$, **b** the average curvature, $\lambda_{1,2}$, of the electron density measured perpendicular to the bond path at $\mathbf{r}_c$, **c** the curvature, λ_3, of the electron density measured parallel to the bond path at $\mathbf{r}_c$, **d** the Laplacian of the electron density, $\nabla^2\rho(\mathbf{r})$, evaluated at $\mathbf{r}_c$, **e** the Brown and Shannon (1973) covalency, f_c, of the MO bonds and **f** the local energy density distribution evaluated at $\mathbf{r}_c$. The *open* and *closed symbols* represent the SiO and GeO data, respectively

number (Table 1). Also, the χ_M-values for Si and Ge calculated for these molecules with Eq. 1 decrease in a regular way with increasing coordination number (denoted by a Roman numeral):

χ_{Si}^{IV}	χ_{Ge}^{IV}	χ_{Si}^{VI}	χ_{Ge}^{VI}	χ_{Si}^{VIII}	χ_{Ge}^{VIII}
1.81	1.83	1.70	1.75	1.46	1.55

In each case, the electronegativity of Ge, rather than being equal to that of Si, is indicated to be ~0.05 larger. Not only does this suggest for a given coordination number that the electronegativity of Ge is larger than that of Si, but it also suggests that the GeO bond is slightly more covalent than the SiO bond, all other things being roughly the same. Silvi et al. (1992) reached a similar conclusion in their study of the valence electrons of the cristobalite modifications of SiO_2 and GeO_2.

From electronegativity considerations (Pauling 1940), the SiO and GeO bonds comprising the tetrahedral MO_4 oxyanions of the H_4MO_4 molecules are indicated to be polar covalent, roughly ~50% ionic, while the character of the MO bonds comprising the octahedral MO_6 oxyanions of the H_8MO_6 molecules is indicated to be roughly 55% ionic; the bonds comprising the cubic MO_8 oxyanion are indicated to be roughly 65% ionic. Thus, as observed for the hydrocarbons, the electronegativities of Si and Ge both decrease with increasing coordination number and decreasing percent s character of the hybrid orbitals primarily because s electrons are lower in energy than p electrons (Allen 1989; Bader 1990). In the case of the SiO and GeO double bonds in the H_2SiO_3 and H_2GeO_3 molecules, the electronegativities of Si (χ_{Si}=1.97) and Ge (χ_{Ge}=1.99) are both ~0.15 larger than the electronegativities of the single bonds of the molecule (χ_{Si}=1.83; χ_{Ge}=1.84). Interestingly, the χ_M-values for the single bonds in the molecule are similar to those in the H_4MO_4 molecules.

Electronegativity variations of Si and Ge with bond critical point properties

As the electronegativities of Si and Ge both increase in value, $\lambda_{1,2}$ decreases (Fig. 3b) while λ_3 (Fig. 3c) and $\nabla^2\rho(\mathbf{r}_c)$ (Fig. 3d) both increase. Thus, with increasing electronegativity (and so with decreasing bond length), the value of the electron density at $\mathbf{r}_c$ increases while the two orthogonal curvatures of $\rho(\mathbf{r}_c)$ perpendicular to the bond and the curvature of $\rho(\mathbf{r}_c)$ parallel to the bond each increase. Inasmuch as λ_3 is appreciably larger than $|\lambda_1|$ and $|\lambda_2|$ and as λ_3 increases at a faster rate than the sum $|\lambda_1+\lambda_2|$ increases, $\nabla^2\rho(\mathbf{r}_c)$ is necessarily positive and increases as the covalent character of the SiO and GeO bond is indicated to increase as observed earlier by Gibbs et al. (1997). This trend is at odds with the results ob-

tained by Bader and Essën (1984) for a set of diatomic hydride molecules where $\nabla^2\rho(\mathbf{r}_c)$ is observed to decrease and to become negative with increasing covalency. This difference may be related to the fact that H has no core electrons inside its valence shell.

The local energy densities, $H(\mathbf{r}_c)$, calculated for SiO and GeO bonds indicate that all of the bonds in Table 1 are covalent bonds. A plot of χ_M versus $H(\mathbf{r}_c)$ shows that $H(\mathbf{r}_c)$ decreases and become more negative as the electronegativities of Si and Ge both increase (Fig. 3f). Also, as $H(\mathbf{r}_c)$ decreases in value, the value of $\rho(\mathbf{r}_c)$ increases with a concomitant stabilization of both bonds and reduction in the local potential energy. On the other hand, Gillespie and Johnson (1997) have recently concluded, on the basis of the 'unexpectedly short' SiO bond length and wide SiOSi angle observed for disiloxane and large atomic charges calculated for Si (+3.05) and O (−1.72) in an integration of the electron density over the basins of the atoms in the molecule (the virial partitioning method of Bader 1990) that the SiO bond is very ionic. However, the magnitudes of the charges obtained by a virial partitioning of the electron density distribution are difficult to interpret and to relate to bond character on an absolute basis. A virial partitioning by Maslen and Spackman (1985) of the promolecule representation of the electron density distribution of the SiO molecule, for example, confers an atomic charge of +1.63 on the Si atom. This is substantially larger than the charge of zero expected for a promolecule for which the charge transfer is zero. Maslen and Spackman (1985) also found that a virial partitioning of the electron density for a large variety of diatomic molecules conferred a substantial transfer of charge, resulting in atomic charges that are substantially larger than those generated with other strategies (Hess et al. 1993), implying an enhanced polarity of the bonds. However, despite the larger transfer of charge, the resulting charges do show sensible correlations with such chemical properties as electronegativity and dipole moment (Maslen and Spackman 1985). Indeed, a knowledge of the charges can be very meaningful and useful in the study of crystals, especially in the study of phase transformations where we would like to have a notion on the action occurring around the individual atoms associated with such reactions.

In an important study of bond-strength bond-length relationships for a large number of oxide crystals, Brown and Shannon (1973) related the resulting strength of an *M*O bond to its covalency, f_c, estimated with the empirical expression of the form $f_c = a(R/R_1)^{-MN_1}$ where R is the length of the bond,

$$f_c'(\mathrm{SiO}) = 0.54(R/1.625)^{-6.48},$$
$$f_c'(\mathrm{GeO}) = 0.60(R/1.750)^{-8.10}.$$

The χ_M-values for Si and Ge (Table 1), plotted against f_c in Fig. 3e, show that both χ_{Si} and χ_{Ge} fall along a single curve with the electronegativities of Si and Ge increasing in regular way as the covalencies of the two bonds are indicated to increase. This trend supports Pauling's (1940) argument that the covalency of an *M*O bond, estimated from the electronegativity difference between atoms *M* and O comprising a coordination polyhedron, is closely related to the mean bond strength of its *M*O bonds (Brown and Shannon 1973). It is also consistent with the observation that the covalent character of the SiO and GeO bonds both increase with decreasing bond length and coordination number. With the observation that his strategy for determining resonance bond numbers for the bonds of organic molecules is equivalent to his strategy for determining electrostatic bond strengths for the bonds in ionic crystals, Pauling (1960) observed in a footnote that the electrostatic bond strength of a bond can be equated with bond number, the greater the strength of a bond, the shorter the bond and the more covalent the bond.

As observed already, the GeOGe angle is, on average, about ∼15° narrower than the SiOSi angle, an observation that has been ascribed in part to the greater electronegativity of the Ge atom and a greater concomitant directionality of the GeO bond. However, a mapping of the (3, −3) critical points in the valence shell concentration of the bridging anions of the molecules $H_6Si_2O_7$ and $H_6Ge_2O_7$ reveals that the bridging anion on the later molecule has two local maxima that can be ascribed to two nonbonded lone electron pairs, whereas that of the former molecule only has one ascribed to one nonbonded electron pair (Bader 1990). According to Gillespie's (1960) VSEPR model, nonbonded electron pairs have larger domains than bonded electron pairs in the same valence shell. The repulsions between the two nonbonded electron pair domains and the two GeO bonded electron pair domains are believed to be greater than those between the one nonbonded electron pair domain and two SiO bonded electron pair domains. Thus, according to the VSEPR model, the $H_6Ge_2O_7$ molecule can be expected to exhibit a narrower bridging angle in minimizing bonded electron pair-nonbonded electron pair repulsions. A similar argument can be used to explain why the SiSSi angle in the $H_6Si_2S_7$ molecule is narrower than the SiOSi angle in the $H_6Si_2O_7$ molecule (Gibbs et al. submitted).

Discussion

The topology of the electron density distributions and the bcp properties of the SiO and GeO bonds are similar, with the electronegativity of Ge indicated to be slightly larger than that of Si as observed by earlier workers (see Allen 1994). From electronegativity considerations, both bonds are indicated to be polar covalent bonds with the covalent character of their bonded interactions increasing with decreasing bond length and coordination number and increasing bond strength. With decreasing bond length and increasing covalent character, the value of $\rho(\mathbf{r}_c)$ and the curvatures perpendicular to the bond path both increase in value in agreement with the B&E bcp criteria. In contrast, however, the curvature at $\mathbf{r}_c$ paralleling the bond path and the Laplacian of $\rho(\mathbf{r}_c)$ are both relatively large and increase in value while the ratio $|\lambda_1|/\lambda_3$ decreases

as the covalent character is indicated to increase. However, if, as done in this study and in the studies completed for the oxides and nitrides, a collection of *M*O bonds is considered for a given *M* cation, then the inherent nature of the electron density distributions of the bonded atoms in the internuclear region virtually guarantees that as $R(MO)$ decreases, $\rho(\mathbf{r}_c)$ and λ_3 must necessarily increase and so the B&E criteria do not apply in these cases. On the other hand, if the bond length is kept fixed but the *M* cation is changed, then the trends appear to be consistent with the criteria (Gibbs et al. 1997; Hill et al. 1997; Feth et al. 1998). Therefore, when applying the B&E criteria, one should consider the impact that a range of bond lengths can have on the bcp properties and the bond types assigned to a set of bonded interaction. On the other hand, C&K criteria that the covalency of a bond increases with decreasing the local energy density is borne out by this study.

The electronegativities obtained from the bcp properties of an *M*O bond are similar to those determined by Pauling and others; they can also be used to provide a rough estimate of bond type as done here and elsewhere for the oxides and nitrides. Also, if the electronegativities provided by the critical point properties of a bond are realistic, then, with a few exceptions involving highly electronegative atoms, as the covalent character of a bond increases, there is a progressive build-up of electron density at the bond critical point coupled with a progressive increase in each of its associated curvatures and its Laplacian. Nevertheless, caution may to be exercised in attaching too much significance to the critical point properties, the electronegativity, classification of bonded interactions and the trends discussed in this report inasmuch as they are determined by the properties of the electron density distribution evaluated at a single point, rather by properties that are evaluated over a more global domain of the electron density distribution.

In conclusion, the similarity of the crystal chemistry and the physical behavior of silicate and germanate materials appears to stem, in part, from the fact that the topography and the topology of the electron density distributions of the SiO and GeO bonds are strikingly similar. This similarity plus the similarity of the total valence electron density distributions calculated for the SiO_2 and GeO_2 modifications of cristobalite (Silvi et al. 1992) provides a basis for understanding why germanates at ambient conditions served as useful high pressure probes for modeling how structurally similar silicates respond to pressure, why silicates and germanates adopt similar crystal structures and why their bond lengths and angles are similarly correlated. This is particularly true when it is recalled that the force field, the force constants and the geometry of a bonded system are closely related to its electron density distribution (Feynman 1939), and that the electron density distribution of a bonded array of atoms incorporates all of the information that embodies the structure, and reactivity of the array (Kraka and Cremer 1990).

Acknowledgements The National Science Foundation is thanked for generously supporting this study with grant EAR-9627458. Professor Dieter Cremer of the University of Göteborg is thanked for his comments on the strengths and weaknesses of the Becke3LYP method and on the applicability of the local energy density criteria to systems whose bonded interactions have a large ionic component. Also, Professor Mark Spackman of the University of New England is thanked for his comments on the partitioning of electron density distributions and the significance and meaning of the resulting charge transfer and atomic charges. In addition, an unknown reviewer made several important suggestions regarding the trends in the bond critical point properties and the classification of bond type that improved the manuscript.

References

Allen LC (1989) Electronegativity is the average one-electron energy of the valence-shell electrons in ground-state free atoms. J Am Chem Soc 111:9003–9014

Allen LC (1994) Chemistry and electronegativity. Int J Quant Chem 49:253–277

Bader RFW (1990) Atoms in molecules Oxford Science Publications Oxford, UK

Bader RFW, Essén H (1984) The characterizations of atomic interactions. J Chem Phys 80:1943–1960

Biegler-König FW, Bader RFW, Tang TH (1982) Calculation of the average properties of atoms in molecules. II. J Comp Chem 13:317–328

Binggeli N, Troullier N, Luís Martins J, Chelikowsky JR (1991) Electronic properties of α-quartz under pressure. Am Phys Soc 44:4771–4777

Boisen MB, Gibbs GV (1987) A method for calculating fractional s-character for bonds of tetrahedral oxyanions in crystals. Phys Chem Min 14:373–376

Boyd RJ, Edgecombe KE (1988) Atomic and group electronegativities from electron density distributions of molecules. J Am Chem Soc 110:4182–4186

Brown GE, Gibbs GV, Ribbe PH (1969) The nature and variation in length of the SiO and AlO bonds in framework silicates. Am Mineral 54:1044–1061

Brown ID, Shannon RD (1973) Empirical bond-strength bond-length curves for oxides. Acta Cryst A29:266-282

Burkhard DJM, DeJong BHWS, Meyer AJHM, Van Lenthe JH (1991) $H_6Si_2O_7$: ab initio molecular orbital calculations show two geometric conformations. Geochim Cosmochim Acta 55: 3453–3458

Cohen RE (1994) First-principle theory of crystalline silica. SILICA. In: Heaney PJ, Prewitt CT, Gibbs GV (eds) Reviews in Mineralogy, Vol. 29, Ch 10, American Mineralogist, Washington, DC 369–402

Cremer D (1987) New ways of analyzing chemical bonding In: Maksicl' ZD (ed) Modelling of structure and properties of molecules. Halsted Press, New York, N. Y., pp 128–144

Cremer D, Kraka E (1984a) Chemical bonds without bonding electron density – does the difference electron-density analysis suffice for a description of the chemical bond? Angew Chem Int Ed Engl 23:627–628

Cremer D, Kraka E (1984b) A description of the chemical bond in terms of local properties of the electron density and energy. Croatia Chemica Acta 57:1259–1281

Cremer D, Gauss J, Cremer E (1988) Strain in three-membered rings containing silicon; the inability of Si to form flexible hybrid orbitals. J Mole Struct 169:531–561

Downs JW (1991) Electrostatic properties of minerals from X-ray diffraction data: a guide for accurate atomistic models. In: Ganguly J (ed) Diffusion, atomic ordering, and mass transport, advances in physical geochemistry, vol 8. Springer-Verlag, Berlin Heidelberg New York

Downs JW (1994) The charge density of coesite. Trans Am Geophys Union Abstr 187

Downs JW (1995) The electron density distribution of coesite. J Phys Chem 99:6849–6856
Downs JW, Swope RJ (1992) The Laplacian of the electron density and the electrostatic potential of danburite, $CaB_2Si_2O_8$. J Phys Chem 96:4834–4840
Downs RT, Gibbs GV, Bartelmehs KL, Boisen MB (1992) Variations of bond lengths and volumes of silicate tetrahedra with temperature. Am Mineral 77:751–757
Feth S, Gibbs GV, Boisen MB, Hill FC (1998) An assessment of the bonded interactions in nitride molecules using bond critical point properties and relative electronegativities. Phys Chem Min 25:234–241
Feynman RP (1939) Forces in molecules. Phys Rev 56:340–343
Foresman JB, Frisch AE (1996) Exploring chemistry with electronic structure methods. Gaussian Inc., Pittsburgh, PA
Frisch MJ, Trucks GW, Schlegel HB, Gill PMW, Johnson BG, Wong MW, Foresman JB, Robb MA, Head-Gordon M, Replogle ES, Gomperts R, Andres JL, Raghavachari K, Binkley JS, Gonzalez C, Martin RL, Fox DJ, Defrees DJ, Baker J, Stewart JJP, Pople JA (1993) Gaussian 92/DFT, Revision F.2 Gaussian Inc., Pittsburgh, PA
Gatti C, Bianchi R, Destro R, Merati F (1992) Experimental vs. theoretical topological properties of charge density distributions. An application to the L-alanine molecule studied by X-ray diffraction at 23 K. J Mole Struct 255:409-433
Gibbs GV (1982) Molecules as models for bonding in silicates. Am Mineral 67:421-450
Gibbs GV, Boisen MB (1998) A molecular modeling of bonded interactions of crystalline.In: Rappaport Z, Apeloigh Y (eds) The chemistry of organicsilicon compounds, vol 2. John Wiley and Sons, New York, N. Y., ch 4
Gibbs GV, Meagher EP, Newton MD, Swanson DK (1981) A comparison of experimental and theoretical bond length and angle variations for minerals, inorganic solids, and molecules In: O'Keeffe M, Navrotsky A (eds) Structure and bonding in crystals vol 1, pp 195–225 Academic Press, New York
Gibbs GV, D'Arco P, Boisen MB (1987) Molecular mimicry of the bond length and angle variations in germanate and thiogermanate crystals: a comparison with variations calculated for carbon-, silicon-, and Sn-containing oxide and sulfide molecules. J Phys Chem 91:5347–5354
Gibbs GV, Downs JW, Boisen MB (1994) The elusive SiO bond SILICA, Reviews in Mineralogy vol 29. Heaney PJ, Prewitt CT, Gibbs GV (eds) American Mineralogist, Washington, DC, pp 331–368
Gibbs GV, Hill FC, Boisen MB (1997) The SiO bond and electron density distributions. Phys Chem Minerals 24:167–178
Gillespie RJ (1960) Bond angles and the spatial correllation of electrons. J Am Chem Soc 82:5978–5983
Gillespie RJ, Johnson SA (1997) Study of bond angles and bond lengths in disiloxane and related molecules in terms of the topology of the electron density and its Laplacian. Inorg Chem 36:3031–3079
Glinnemann J, King HE, Schulz H, Hahn T, Placa SJ, Dacol F (1992) Crystal structures of the low-temperature quartz-type phases of SiO_2 and GeO_2 at elevated pressure. Z Kristallogr 198:177–212
Goldsmith JR (1950) Gallium and germanium substitutions in synthetic feldspar. J Geol 58:518–536
Goldschmidt VM (1931) Crystal chemistry of germanium. Nachr Ges Wiss Göttingen Math Physik Kl 184:190
Hess B, Lin HL, Niu JE, Schwartz WHE (1993) Electron density distributions and atomic charges. Z Naturforsch 48a:180–192
Hill FC, Gibbs GV, Boisen MB (1994) Bond stretching force constants and compressibilities of nitride, oxide and sulfide coordination polyhedra in molecules and crystals. Struct Chem 5:349–354
Hill FC, Gibbs GV, Boisen MB (1997) Electron density distributions of oxide and hydroxyacid molecules. Phys Chem Min 24
Hill RJ, Louisnathan SJ, Gibbs GV (1977) Tetrahedral bond length and angle variations in germanates. Aust J Chem 30:1673-1684
Jackson MD, Gibbs GV (1988) A modeling of the coesite and feldspar framework structure types of silica as a function of pressure using MEG methods. J Phys Chem 92:540–545
Kraka E, Cremer D (1990) Chemical implications of local features of the electron density distributions. In: Maskíc ZB (ed) The concept of the chemical bond. Springer-Verlag, Berlin Heidelberg New york, pp 457–544.
Maslen EN, Spackman MA (1985) Atomic charges and electron density partitioning. Aust J Phys 38:273–287
MacDougal PJ (1989) The Laplacian of the electron density distribution. Doctoral Thesis, Chemistry Department, McMaster University, Hamiliton, Ontario, Canada
McCormack GR (1964) The system magnesia-magnesium fluoride-germania lithium fluoride. Bureau Mines Report Invest 63:981–11
McCormack GR (1966) Subsolidus equilibria in the system MgO–-GeO–MgF_2. J Am Ceram Soc 49:618–620
McCormack GR Ehlers EG (1967) Ternary phases in the system MgO–GeO_2-LiF. J Am Ceram Soc 50:439–440
Miller JL, McCormack GR, Ampian SG (1967) Phase equilibria in the system GeO_2–Al_2O_3. J Am Ceram Soc 50:268–269
Navrotsky A (1989) Silicates and germanates at high pressures. In: Wittingham MS, Bernasek S, Jacobson AJ, Navrotsky A, (eds) Reactivity of Solids, North Holland, Amsterdam 288–297
Navrotsky A (1989) Silicates and germanates at high pressures. Solid State Ionics, Diffusion and reactions 32:288–297
Neuefeind J, Liss KD (1996) Bond angle distribution in amorphous germania and silica. Ber Bunsenges Phys Chem 100:1341–1349
Nishi F, Takéuchi Y (1992) The nature of the variation of Ge–O bonding in germanates. Z Kristallogr 202:251–259
Pauling L (1940) The nature of the chemical bond, 2nd edn. Cornell University Press Ithaca, NY
Pauling L (1960) The nature of the chemical bond, 3rd edn. Cornell University Press Ithaca, NY
Shannon RD, Prewitt CT (1969) Effective ionic radii in oxides and fluorides. Acta Cryst B25:925–946
Silvi B, Allavena M, Hannachi Y, D'Arco P (1992) Pseudopotential periodic Hartree-Fock study of the cristobalite phases of silica and germanium oxide. J Am Chem Soc 75:1239–1246
Smrĉok L, Benco L̂ (1996) Ab initio periodic Hartree-Fock study of lizardite 1*T*. Am Mineral 81:1405–1412
Spackman MA, Maslen EN (1985) Electron density and the chemical bond. Reappraisal of Berlin's theorem. Acta Crystallogr A41:347–353
Stuckenschmidt E, Joswig W, Baur WH (1994) Natrolite. Part II: determination of the deformation electron densities by X–X method. Phys Chem Minerals 21:309–316
Teppen BJ, Miller DM, Newton SQ, Schäfer L (1994) Choice of computational techniques and molecular models for *ab initio* calculations. J Phys Chem 98:12545–12557
Tossell JA, Gibbs GV (1978) The use of molecular-orbital calculations on model systems for the prediction of bridging-bond variations in siloxanes, silicates, silicon nitrides and silicon sulfides. Acta Crystallogr A34:463–472
Toraya H, Iwai S, Marumo F (1978) The crystal structures of germanate micas, $KMg_{2.5}Ge_4O_{10}F_2$ and $KLiMg_2Ge_4O_{10}F_2$. Z Kristallogr 148:65–81
Tsirelson VG, Evdokimova OA, Belokoneva EL, Urusov VS (1990) Electron density distribution and bonding in silicates: a review of recent data. Phys Chem Minerals 17:275–292
Weber JN (1973) Editor's comments on papers 1 through 6 Geochemistry of germanium. In: Weber JN (ed.) Benchmark papers in geology. Dowden, Hutchingson and Ross, Stroudsburg, PA